Available online at www.sciencedirect.com

ScienceDirect

Nuclear and Particle Physics Proceedings 267–269 (2015) 43–47

www.elsevier.com/locate/nppp

Search for a Higgs Boson decaying to $\gamma\gamma^* \to \gamma\ell^+\ell^-$ in pp collision at $\sqrt{s} = 8$ TeV at the CMS experiment

Luisa Fernanda Chaparro Sierra[a]

[a] *Universidad de Los Andes, Carrera 1 18A-10, Bloque Ip. Bogotá - Colombia. A.A. 4976-12340*

Abstract

The results of the Standard Model Higgs boson decay into a real photon and a virtual photon ($\gamma\gamma^*$) are presented. The analysis is performed using proton-proton collision data recorded by the CMS detector at the LHC. The events were collected at 8 TeV center-of-mass energy. No excess of events above background is found in the 120 – 150 GeV Higgs boson mass range.

Keywords: Higgs boson, Proton-proton collision, CMS Experiment, LHC.

1. Introduction

The rare Higgs boson decay into the $\mu\mu\gamma$ final state features a high information content that can potentially give point to extensions of the standard model (SM) [1], since the decay is sensitive to new-physics through its loop structure. The decay takes the name "Dalitz" in analogy with the $\pi^0 \to ee\gamma$ decay. The SM Dalitz decay proceeds via a conversion of one of the photons into a pair of leptons $H \to \gamma\gamma^* \to \gamma\ell\ell$. In this analysis only the case of muons is considered.

The $H \to \gamma\gamma^* \to \gamma\mu^+\mu^-$ channel is mixed with the $H \to \gamma Z \to \gamma\mu^+\mu^-$ channel since both, γ and Z, are neutral vector bosons that can coupled to the pair of muons. The main contributions to this channel are loop-induced processes, but tree-level diagrams with initial-state and final-state radiation, such as $H \to \mu\mu$ and $H \to q\bar{q}$, where $q\bar{q}$ hadronizes into mesons which decay to $\mu\mu$ also contribute. Other high-order box diagrams have negligible contributions (See Fig.1).

The Higgs boson branching fraction to $\mu\mu\gamma$ is dominated by the Dalitz and $Z\gamma$ modes when the invariant mass of the dimuon is less than 100 GeV. At higher invariant mass, final state radiation plus $H \to \mu\mu$ dominates. As illustrated in Fig.2, the Dalitz mode dominates the region below 20 GeV in the dimuon invariant mass; the $Z\gamma$ mode dominates in the region around 80 GeV. The region between 20 and 50 GeV corresponds to an interference between Dalitz and $Z\gamma$ modes. For this reason, requirements on the dimuon invariant mass ($m_{\mu\mu}$) and transverse momentum of the photon are used to separate $H \to \gamma^*\gamma$ and $H \to Z\gamma$.

In order to isolate the contribution from the Dalitz decay, the analysis is limited to the phase space region defined by $m_{\mu\mu} < 20$ GeV and a transverse momentum (p_T) for the photon of at least 40 GeV. From Fig 2, at very low dilepton mass, the muons tend to be close to each other ($\Delta R \to 0$), a relatively high energy photon in the opposite direction and a 3-body invariant mass, consistent with the mass of the Higgs boson candidate.

The main backgrounds are:

- Irreducible contribution from the initial-state radiation in muon Drell-Yan production.
- Final-state photon radiation, mostly from Z decays.
- Muon Drell-Yan production with additional jets, where one of the jets is misidentified as a photon.

http://dx.doi.org/10.1016/j.nuclphysbps.2015.10.080

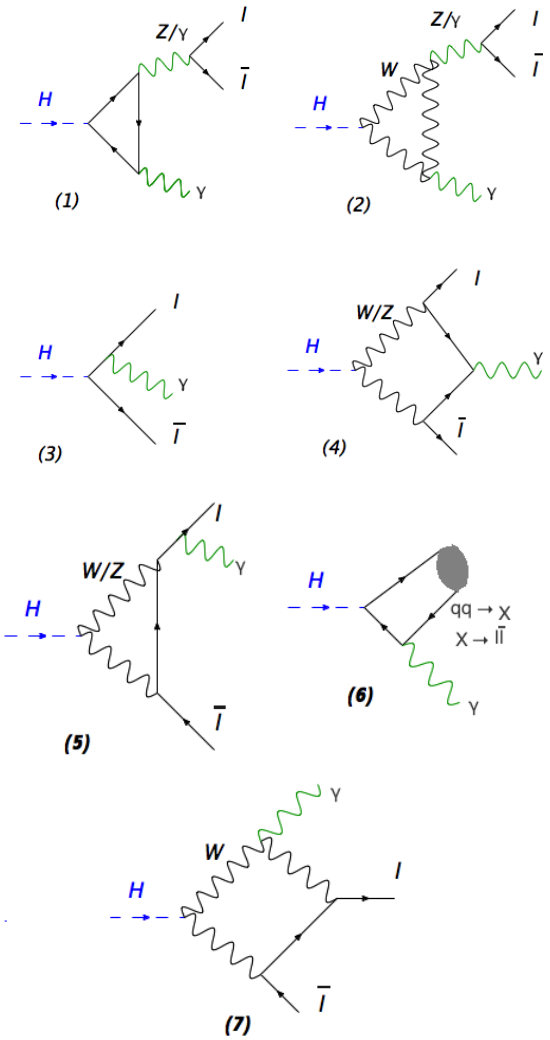

Figure 1: Diagrams contributing to $H \to \mu\mu\gamma$. The contributions from diagrams (1) and (2) dominate. The final state-radiation (3) contribution, is important at high dilepton invariant mass. Contributions from resonances (6) can be identified using the dilepton mass information. The contributions from (4), (5) and (7) are negligible.

The results presented here are based on proton-proton collision data recorded by the CMS detector at the LHC at $\sqrt{s} = 8$ TeV, corresponding to an integrated luminosity of 19.7 fb^{-1}.

2. The CMS detector

The central feature of the CMS apparatus is a superconducting solenoid of 6 m internal diameter, providing a magnetic field of 3.8 T. Within the superconducting solenoid volume are a silicon pixel and strip tracker, a lead tungstate crystal electromagnetic

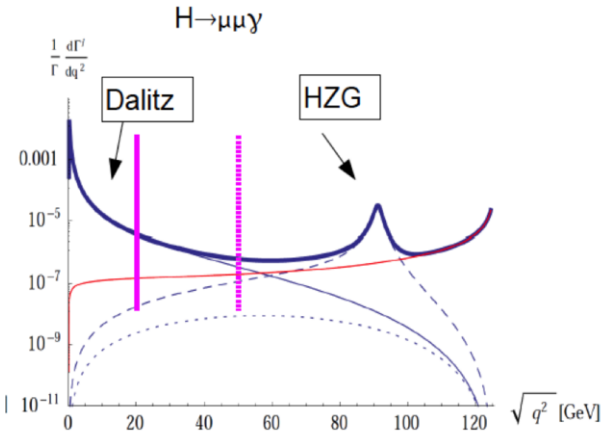

Figure 2: Dilepton invariant mass. The red line denotes the contribution of the tree-diagrams. The thin solid line denotes the contribution from the γ^* pole diagrams. The dashed line shows the contribution from the Z^* pole diagrams, while dotted line denotes the contribution from the four-point box diagrams. The thick line gives the total contributions. Taken from Ref. [1]

calorimeter (ECAL), and a brass and scintillator hadron calorimeter (HCAL), each composed of a barrel and two endcap sections. They provide measurements of the energy of photons, electrons and jets. Muons are detected in gas-ionization detectors embedded in the steel flux-return yoke outside the solenoid. Extensive forward calorimetry complements the coverage provided by the barrel and endcap detectors. For this analysis the information for the reconstruction of photons comes mostly from the electromagnetic calorimeter; in the case of the reconstruction of muons, the muon system in combination with the inner tracker and the calorimeters is used. A detailed description of the CMS detector can be found in Ref. [2].

3. Event selection

For this analysis the events were required to pass a high level trigger, that demand a photon and a muon with a $p_T > 22$ GeV. Events with two opposite-sign muons and a photon are selected: $\mu^+\mu^-\gamma$. For muons, the requirement for pseudorapidity (η) is less than 2.4, while for the photon, $|\eta| < 1.44$ is required. All particles must be isolated and have traverse momentum greater than 23 GeV for the highest-p_T lepton and greater than 4 GeV for next to the highest-p_T lepton, $p_T^\gamma/m_{\mu\mu\gamma} > 0.3$ for the photon and $p_T^{\mu\mu}/m_{\mu\mu\gamma} > 0.3$ for the muon pair. The transverse momentum requirement on the highest-p_T muon is driven by the trigger threshold

and on the next to highest-p_T by the minimum energy needed to reach the muon system. The photon threshold is optimized for high signal efficiency and background rejection. The dilepton invariant mass ($m_{\mu\mu}$) is required to be less than 20 GeV in order to reject contributions from $pp \to \gamma Z$ and $H \to \gamma Z$. The mass window for the system $\mu^+\mu^-\gamma$, is required to be between 110 and 170 GeV.

The events are required to have at least one primary vertex. In the case of multiple reconstructed vertices associated with additional interactions (pileup), the one with the highest scalar sum of the p_T^2 of its associated tracks is chosen as primary vertex. The leptons are required to originate from the primary vertex.

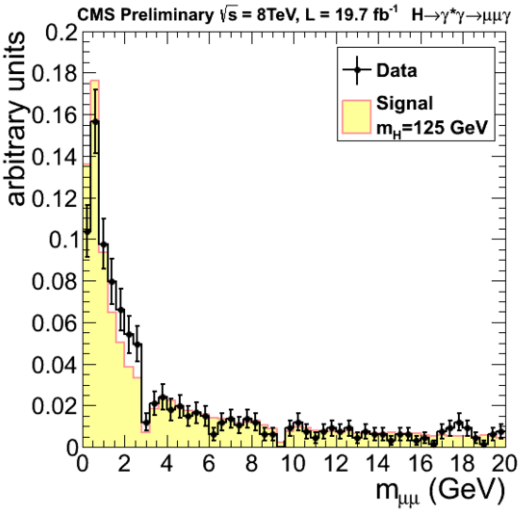

Figure 3: Dilepton invariant mass, $m_{\mu\mu}$. Points with error bars denotes data, and simulated SM Higgs boson signal events, $m_H = 125$ GeV, (histogram)

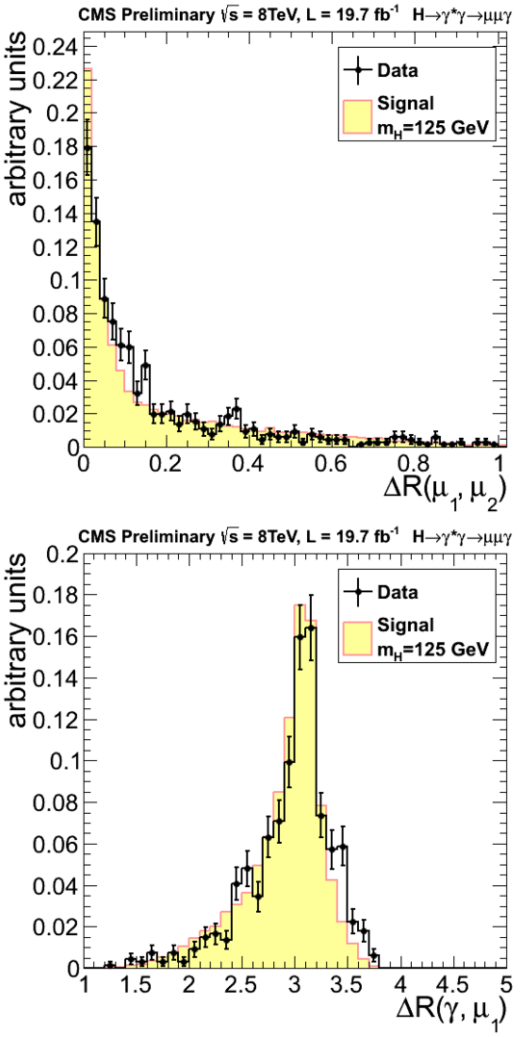

Figure 4: Separation between the two muons, $\Delta R(\mu_1\mu_2)$ (up), the individual muons and the photon, $\Delta R(\gamma\mu_1)$ (down). Points with error bars denotes data, and simulated SM Higgs boson signal events, $m_H = 125$ GeV, (histogram)

The observables used in the photon selection are:

- Isolation variables based on the particle-flow algorithm (PF) [3].
- The ratio between energy in the hadron calorimeter towers behind the supercluster and the electromagnetic energy in the supercluster.
- The transverse width in η of the electromagnetic shower.
- A pixel tracker veto to avoid misidentifying an electron as a photon.

Muon candidates are reconstructed with the tracker and identified with the PF algorithm using hits in the tracker and the muon system. Muons from internal conversions are expected to be isolated from other particles, but their separation, ΔR, is small due to the low invariant mass of the dimuon, see Fig 4 (Upper plot). With all these requirements the combined identification and isolation efficiencies are of the order of 90%.

Events with dilepton mass between 2.9 GeV and 3.3 GeV as well as events with dilepton mass between 9.3 and 9.7 GeV are rejected to avoid J/Ψ and Υ contributions respectively. If two dilepton pairs are present, the pair with the lowest dilepton invariant mass is chosen. Finally, the dilepton and the photon must be ”back-to-

back". The ΔR separation between each lepton and the photon must be greater than 1.0 in order to suppress events with final state-radiation (Drell-Yan or Z decays).

The three-body mass spectrum and the transverse momentum for the muons and the photon, after the final selection, are shown in Figs. 5, 6 and 7. The shape of the signal and the data, which is around to 100% background, is very similar for most of the distributions (Figs 3-5). This feature makes this analysis a challenge.

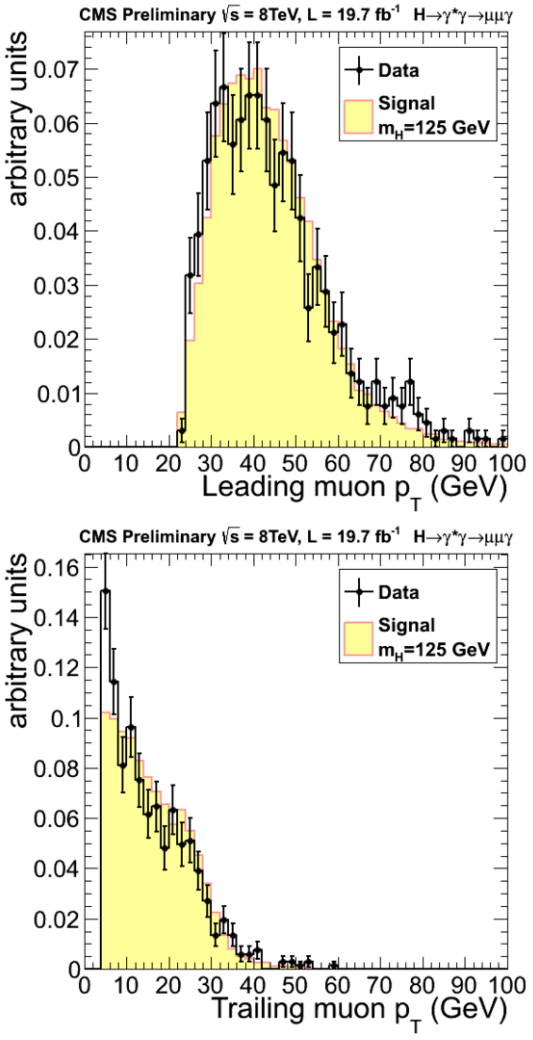

Figure 5: Transverse momentum for the muons (middle, down) for data (points with error bars), and simulated SM Higgs boson signal events, m_H = 125 GeV, (histogram).

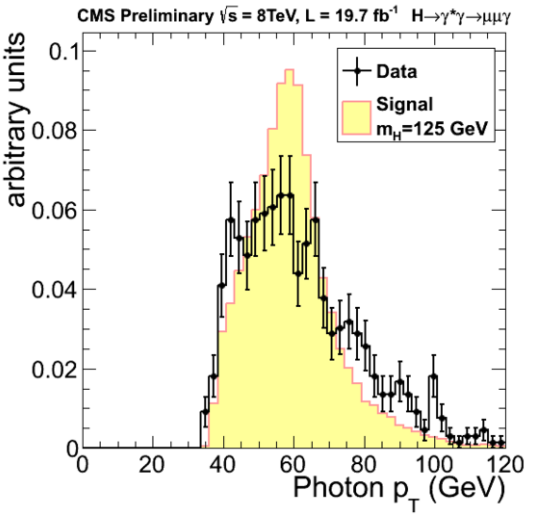

Figure 6: Transverse momentum for the photon (up) for data (points with error bars), and simulated SM Higgs boson signal events, m_H = 125 GeV, (histogram)

4. Background and signal modeling

The background model is obtained by fitting the observed $\mu\mu\gamma$ mass distribution. The fitting is unbinned and is performed over the three body invariant mass range of 110-170 GeV. This spectrum is a falling distribution that is fitted to a polynomial. The background fit based on the $m_{\mu\mu\gamma}$ is shown in Fig. 7. The potential bias on the background measurement is studied by using pseudo-data generated from background-only fits to the observed three-body mass spectrum. These pseudo-data sets are fitted to a signal combined with a polynomial background model. The results of these fits are used to determine the polynomial degree for the background model. A fourth order polynomial was used to fit the data.

The description of the Higgs boson signal used in the search is obtained from simulated events produced at leading-order using the Madgraph 5 [4] interfaced with PYTHIA 6.4 [5] for the gluon-gluon fusion, vector boson fusion and associated production with a vector boson processes. The parton distribution functions (PDF) used to produce these samples are those of CT10 [6]. The branching fractions are estimated using MCFM [7]. The SM Higgs boson cross sections are taken from Refs [8, 9]. The signal model is obtained form an unbinned fit to the mass distribution of the simulated events to the Crystal Ball function [10] and a Gaussian.

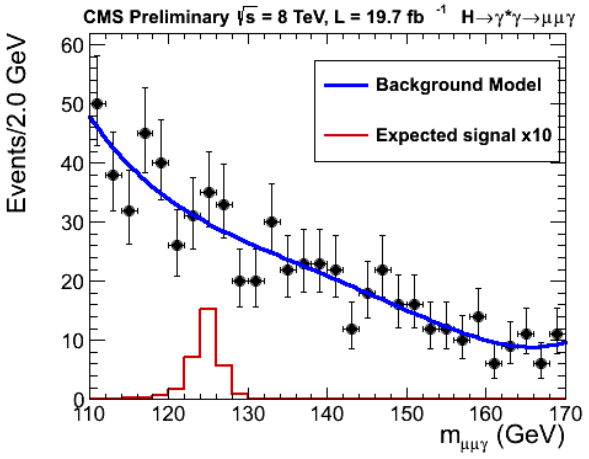

Figure 7: The $m_{\mu\mu\gamma}$ spectrum for 8TeV data (points with error bars). Also shown is the simulated SM Higgs boson signal events, $m_H = 125GeV$ (histogram) scaled by 10.

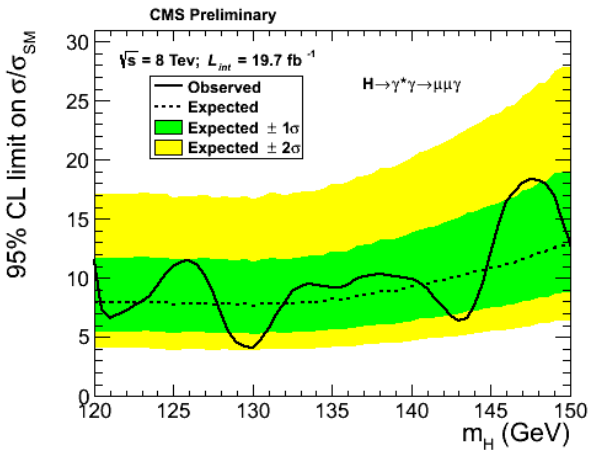

Figure 8: The exclusion limit as a function of the mass hypothesis, m_H, on te cross section times the branching fraction of a Higgs boson decaying into a photon and a muon pair with dilepton mass less than 20 GeV divided by the SM value.

The simulated events are weighted by scale factors to take into account the difference with the data. The factors are:

- The distribution of reconstructed vertices.
- The trigger efficiencies.
- The energy and momentum resolution.
- The energy scale.
- The reconstruction and identification efficiency.
- The isolation efficiency observed in data.

5. Results

A statistical analysis to test the significance of any potential signal-like excess is performed in terms of the local p-value. No significant excess of events above background is observed, with a maximum value of less than two standard deviations in the full mass range. For the calculation of exclusion limits, a modified frequentist criterion CL_s was adopted. [11]. The uncertainty on the limit is dominated by the data sample size.

The expected and observed limits are shown in Fig 8. The limits are calculated at 0.5 GeV intervals in the 120-150 GeV mass range. The expected exclusion limits at 95% confidence level are between 8 and 13 times the SM cross section and the observed limit ranges between about 4 and 19 times the SM cross section. The observed and expected limits for the three-body mass ($m_{\mu\mu\gamma}$) at 125 GeV and dilepton mass ($m_{\mu\mu}$) less than 20 GeV are about ten times of the SM prediction.

References

[1] Y. Sun, H. R. Chang, D. N. Gao, Higgs decays to gamma l+ l- in the standard model, JHEP 1305 (2013) 061. arXiv:1303.2230, doi:10.1007/JHEP05(2013)061.
[2] S. Chatrchyan, et al., The CMS experiment at the CERN LHC, JINST 3 (2008) S08004. doi:10.1088/1748-0221/3/08/S08004.
[3] Particle-Flow Event Reconstruction in CMS and Performance for Jets, Taus, and MET, Tech. Rep. CMS-PAS-PFT-09-001, CERN, 2009. Geneva (Apr 2009).
[4] T. Corbett, O. J. P. Éboli, J. Gonzalez-Fraile, M. C. Gonzalez-Garcia, Constraining anomalous higgs boson interactions, Phys. Rev. D 86 (2012) 075013. doi:10.1103/PhysRevD.86.075013.
[5] T. Sjostrand, S. Mrenna, P. Z. Skands, PYTHIA 6.4 Physics and Manual, JHEP 0605 (2006) 026. arXiv:hep-ph/0603175, doi:10.1088/1126-6708/2006/05/026.
[6] M. Guzzi, P. Nadolsky, E. Berger, H.-L. Lai, F. Olness, et al., CT10 parton distributions and other developments in the global QCD analysisarXiv:1101.0561.
[7] J. M. Campbell, R. Ellis, MCFM for the Tevatron and the LHC, Nucl.Phys.Proc.Suppl. 205-206 (2010) 10–15. arXiv:1007.3492, doi:10.1016/j.nuclphysbps.2010.08.011.
[8] S. Dittmaier, et al., Handbook of LHC Higgs Cross Sections: 1. Inclusive ObservablesarXiv:1101.0593, doi:10.5170/CERN-2011-002.
[9] A. Denner, S. Heinemeyer, I. Puljak, D. Rebuzzi, M. Spira, Standard model higgs-boson branching ratios with uncertainties, The European Physical Journal C 71 (9). doi:10.1140/epjc/s10052-011-1753-8.
[10] T. Skwarnicki, A study of the radiative cascade transitions between the upsilon-prime and upsilon resonances, Ph.D. thesis, Cracow TU, Hamburg, presented on Feb 1986 (1986).
[11] T. Junk, Confidence level computation for combining searches with small statistics, Nuclear Instruments and Methods in Physics Research Section A: Accelerators, Spectrometers, Detectors and Associated Equipment 434 (23) (1999) 435 – 443. doi:http://dx.doi.org/10.1016/S0168-9002(99)00498-2.